Room Temperature Wafer-Scale Synthesis of Highly Transparent, Conductive CuS Nanosheet Films via a Simple Sulfur Adsorption-Corrosion Method

John Hong[a,b,†], Byung-Sung Kim[a,†], Bo Hou[c,†], Sangyeon Pak[d], Taehun Kim[d], A-Rang Jang[e], Yuljae Cho[f], Sanghyo Lee[c], Geon-Hyoung An[g], Jae Eun Jang[h], Stephen M. Morris[a], Jung Inn Sohn[i], SeungNam Cha[d,]*

[a] Department of Engineering Science, University of Oxford, Oxford, OX1 3PJ, United Kingdom.

[b] School of Materials Science and Engineering, Kookmin University, Seoul, 02707, Republic of Korea

[c] Electrical Engineering Division, Department of Engineering, University of Cambridge, 9 JJ Thomson Avenue, Cambridge, CB3 0FA, United Kingdom.

[d] Department of Physics, Sungkyunkwan University, Suwon, 16419, Republic of Korea

[e] Department of Electrical Engineering, Semyung University, 65 Semyung-ro, Chungcheongbuk-do 27136, Republic of Korea

[f] University of Michigan – Shanghai Jiao Tong University Joint Institute, Shanghai Jiao Tong University, 800 Dong Chuan Road, Minghang District, Shanghai 200240, China

[g] Department of Energy Engineering, Gyeongnam National University of Science and Technology (GNUST), Jinju, 52725, South Korea

[h] Department of Information and Communication Engineering, Daegu Gyeongbuk Institute of Science and Technology (DGIST), Daegu, 49288, Republic of Korea.

[i] Division of Physics and Semiconductor Science, Dongguk University-Seoul, Seoul, 04620, Republic of Korea.

Keywords: transparent conductive electrodes, transition metal sulfide, vapour corrosion, scalable fabrication, flexible electronics, adsorption isotherm

ABSTRACT

The development of highly conductive electrodes with robust mechanical durability and clear transmittance in the visible to IR spectral range are of great importance for future wearable/flexible electronic applications. In particular, low resistivity, robust flexibility, and wide spectral transparency have a significant impact on optoelectronic performance. Herein, we introduce a new class of covellite copper monosulfide (CuS) nanosheet films as a promising candidate for soft transparent conductive electrodes (TCE). An atmospheric sulfur adsorption-corrosion phenomenon represents a key approach in our work for the achievement of wafer-scale CuS nanosheet films through systematical control of the neat Cu layer thickness ranging from 2 nm to 10 nm multilayers at room temperature. These nanosheet films provide outstanding conductivity (~ 25 Ω sq^{-1}) and high transparency (> 80 %) in the visible to infrared region as well as distinct flexibility and long stability under air exposure, yielding a high figure-of-merit (FoM) (~ 60) that is comparable to that of conventional rigid metal oxide material-based TCEs. Our unique room temperature synthesis process delivers high quality CuS nanosheets on any arbitrary substrates in a short time (< 1 min) scale, thus guaranteeing the widespread use of highly producible and scalable device fabrication.

■ INTRODUCTION

Following the experimental observation of highly conductive graphene, ultrathin two-dimensional (2D) materials, such as transition metal chalcogenides, black phosphorous, boron nitride, or MXenes, have also become promising alternatives for modern technological applications due to their extraordinary physical and mechanical properties at extremely low dimensions.[1-7] In particular, metallic 2D materials have the potential to be a new class of flexible transparent conductive electrodes (TCEs) and could be a key enabling technology in the development of next-generation flexible electronic applications such as smartphones, touch-screens, and display panels, thereby displacing the traditional transition metal oxide materials in terms of flexibility and IR transparency.[8] Of the numerous TCEs currently available, only graphene has been considered as a promising candidate owing to its remarkable electrical and optical properties even though there have been rapid developments in metallic 2D materials.[9-11] This is because there is still much to be done before these metallic 2D materials can be employed as a practical TCE. For example, the preparation of 2D materials frequently require high vacuum and high-temperature synthesis procedures (e.g. chemical vapor deposition),[12-13] inherently limiting the widespread use of these materials grown directly on any polymer-based flexible substrates. Thus, one of the most essential approaches was to select dry or wet transfer processes (e.g from silicon to polymer substrates after synthesis). However, these techniques have significant disadvantages in terms of unintentionally introducing surface defects and wrinkles, which negatively affect the electrical and optical features.[14] Therefore, finding a practical synthetic route that negates the need for additional high-temperature steps and transfer processes remains a key challenge that needs to be solved before these new metallic 2D materials can be deployed in diverse flexible and transparent electronics.

To date, copper sulfides (Cu_xS) of II-VI chalcogenide materials are understood to exhibit a variety of binary phases including Cu_2S (chalcocite), $Cu_{1.96}S$ (djurlite), $Cu_{1.8}S$ (digenite), $Cu_{1.75}S$ (anilite), and CuS (covellite), depending on the copper stoichiometry ($1<x<2$).[15-18] It is widely believed that copper vacancies in copper sulfide compounds are strongly linked with the diverse and unique optoelectronic characteristics that have been widely studied for a range of applications, such as solar cells, electromagnetic shielding layers, functional catalysts, ionic conductors, and superconductors. Among them, the copper-deficient copper monosulfide (CuS) material shows particular promise as an impressive metallic candidate for various applications.[19-22] Theoretical studies indicate that the CuS possesses a graphene-like crystal structure with a P63/mmc space group and highly metallic conductivity perpendicular to the c-axis direction. Despite the large body of work on CuS nanosheets, there are still limitations with regards to the use of low temperature fabrication procedures, the scability of CuS nanosheet films, controlling the thickness and achieving high conductivity values close to the theoretical limit. In fact, overcoming these limitations is essential for their practical realization as a TCE candidate. In addition, finding a new synthetic procedure that results in the tailoring of the CuS composition is challenging due to its stoichiometry-dependent properties.

Herein, we introduce a wafer-scale synthesis method of highly crystalline CuS nanosheet films which has the potential to be an alternative TCE by employing an atmospheric sulfur adsorption-corrosion reaction approach at room temperature (RT). Specifically, the high anion reactive ability of copper transition metals with oxygen or sulfur atoms even at RT ensures the synthesis of high quality, uniform, and ultra-thin CuS nanosheet films (NF) in the range of 2 to 10 nm. The CuS nanosheets exhibit not only a low sheet resistance of ~ 25 Ω sq^{-1} but also excellent optical transparency in the visible to infrared (IR) region of ~ 80%, which is much more transparent

than conventional oxide films in this region of the spectrum.[23] The calculated figure-of-merit (FoM) is found to reach values of ~ 60, which is beyond the minimum industrial requirement for practical applications. Remarkably, these TCE parameters can be preserved even when subjected to large strains, which is particularly important for future flexible electronics. Thus, this simple room temperature chemical deposition process could be generalized and extended towards highly uniform and large scale CuS NFs on any arbitrary substrate for advanced flexible optoelectronic devices, including a promising TCE candidate that could be deployed in various electronic applications (IR device and quantum dot light emitting diodes).

■ RESULTS AND DISCUSSIONS

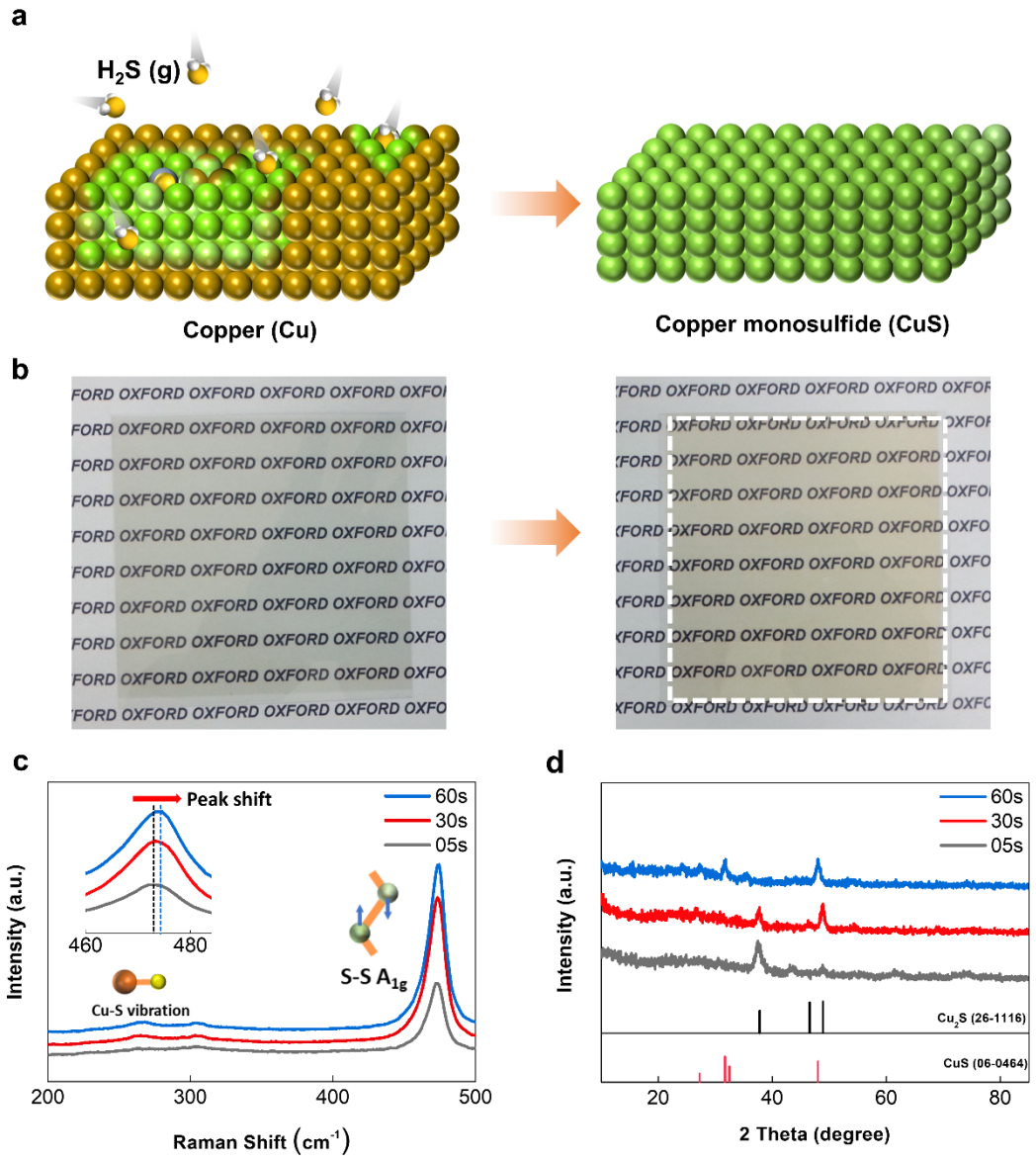

Figure 1. (a) Schematic illustration of the sulfurization process in the CuS nanosheets. (b) Optical images of a 2 nm-Cu nanosheet film and the corresponding CuS nanosheet films before and after the sulfurization process. (c) Raman spectra of the CuS samples after sulfurization process for different time durations (5 sec, 30 sec and 60 sec). (d) XRD results from CuS samples for different duration times (5 sec, 30 sec and 60 sec).

A schematic illustration of the fabrication procedure is shown in **Figure** 1a. A facile, one-step sulfurization method was used to fabricate conductive and transparent CuS nanosheets. Before the sulfurization process, the Cu metal thin nanosheets were carefully deposited on target substrates (glass or PET (polyethylene terephthalate)) by a simple evaporation technique. The thickness of Cu (ranging from ~ 2 to 10 nm) was precisely controlled by the evaporation time. Subsequently, the Cu metal films were directly exposed to H_2S gas that was evaporated from the ammonium sulfide solution. The continuous sulfur supply from the solution readily transforms the pure Cu films into transparent CuS nanosheet films at room temperature (**Figure** 1b). As reported in the literature, chalcocite Cu_2S and covellite CuS are both harvestable phases at room temperature, but the formation of Cu_2S in bulk form has mainly been reported only in sulfur-limiting environments.[24] In contrast to the bulk, the adequate supply of sulfur onto limited Cu dimensions (nm thickness) plays a critical role in forming the covellite CuS phase instead of Cu_2S. The overall atmospheric sulfurization in the presence of H_2S gas take places according to the following reaction:[25]

$$H_2S + 2Cu + 1/2O_2 \rightarrow Cu_2S + H_2O \qquad (1)$$

Usually, highly reactive H_2S can be adsorbed onto a Cu surface, resulting in Cu_2S as the main corrosion product. Moreover, the reaction of sulfur ions at the gas/sulfide interface results in the depletion of cuprous vacancies, which transport through the sulfide layer during the growth of the Cu_2S phase.[26,27] However, it was found that further reaction with the continuous sulfur supply from a gas atmosphere leads to the top layer being converted to the covellite CuS phase. This can be further confirmed by the sulfurization of a Cu foil with the sulfurization process (**Figure** S1). As shown in **Figure** S1a, different exposure times to the sulfur gas induces different surface conditions on the Cu foil with different color changes. Within 5 to 30 sec sulfurization time, most

of the surface of the Cu foil is conjugated with the Cu_2S phase. After 60 sec, the surface turned into the blueish CuS phase. To check the surface states along with a small depth of the Cu foil, the thin nanosheets from the reacted Cu foil were cleaved and transferred to a SiO_2 wafer (**Figure** S1b) via a wet-transfer process. **Figure** S1c shows the optical image of the transferred CuS nanosheets from the Cu foil. Raman analysis was carried out to check the transferred CuS nanosheets, and the peak of the in-plane Cu-S vibration at 266 cm^{-1} for CuS crystal, ensuring the successful conversion of Cu or Cu_2S under the sufficient supply of sulfur gas.[28,29] In addition, measurements from time-of-flight secondary-ion mass spectrometry (TOF-SIMS) suggests the fast out-diffusion of the cuprous vacancy and sulfur atom on the Cu foil for short timescales (< 1 min) even at room temperature (**Figure** S2a).

To investigate the phase-transition mechanism in the CuS samples, Raman and XRD (X-Ray Diffraction) measurements were systematically carried out with 10 nm-Cu nanosheets for different sulfurization times. A dominant peak at 472 cm^{-1} for the Cu film exposed for 5 sec was identified to be the Cu_2S phase, which gradually shifted to 474 cm^{-1} corresponding to the out-of-plane S-S vibration (A_{1g} mode) in the covellite CuS phase (**Figure** 1c and inset).[30] The peak of the in-plane Cu-S vibration at 266 cm^{-1} is also intensified according to an increased sulfurization time (**Figure** S2b and 2c**).** The peak shifts at 474 cm^{-1} as well as the enhanced peak intensity at 266 cm^{-1} indicate that with the appropriate supply of sulfur to the limited Cu dimensions is a key parameter in generating covellite CuS from Cu sources. To further support our proposed mechanism, XRD measurements for the corresponding sulfurization times and a similar variation tendency (**Figure** 1d and **Figure** S2d**)** was conducted. The results also demonstrate the successful transition from cubic Cu (JCPDS Card No. 85-1326) and chalcocite Cu_2S (JCPDS Card No. 26-1116) to covellite CuS (JCPDS Card No. 06-0464) at room temperature after longer sulfurization times.[31,32]

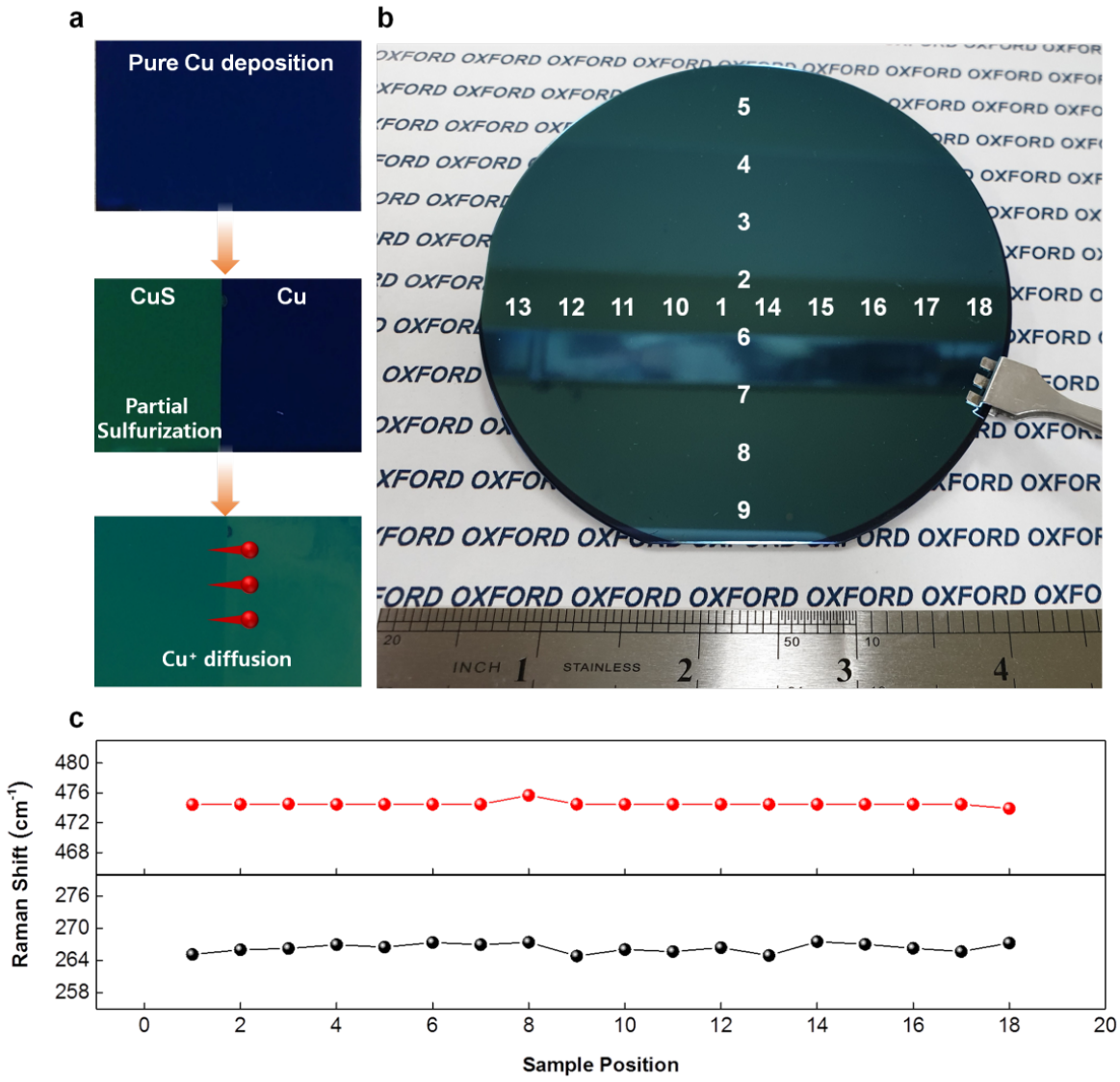

Figure 2. (a) Lateral sulfur diffusion in Cu/CuS nanosheet films. (b) Large scale fabrication of a CuS nanosheet on a SiO_2/Si substrate. (c) Raman shifts at selected points across the sample as labelled in **Figure** 2b.

As shown in **Figure** 2a, 10 nm-Cu films were deposited onto a SiO_2 substrate and the partial area of the deposited Cu films was initiated via a sulfurization process. The straight line in the

optical image represents the boundary between the Cu and CuS films. After a few hours, an area of the Cu film on the boundary line was also converted into CuS. This is due to the high sulfur and cuprous Cu diffusivity from the localized sulfur atoms. Based on the scalable and facile vapor-based sulfurization method and diffusion of cuprous Cu and S, large wafer-scale CuS nanosheet films can also be successfully synthesized on a 4-inch scale Si wafer (**Figure** 2b). The as-grown CuS nanosheets were continuously and uniformly fabricated over a large area of the Si wafer. **Figure** 2c exhibits the representative Raman spectrum analyses on the randomly selected 18 different points on the CuS samples in order to quantitatively confirm the uniformity over a large area. As seen, the peak positions of the S-S (A1g mode) and Cu-S modes remain identical in all the spectra, which are centered at ~474 cm^{-1} and ~ 266 cm^{-1}, respectively, confirming the excellent uniformity of CuS on the substrate. **Figure** S3 shows the areal AFM scanning image, which indicates a uniform surface of 10 nm-CuS on the SiO_2 substrate.

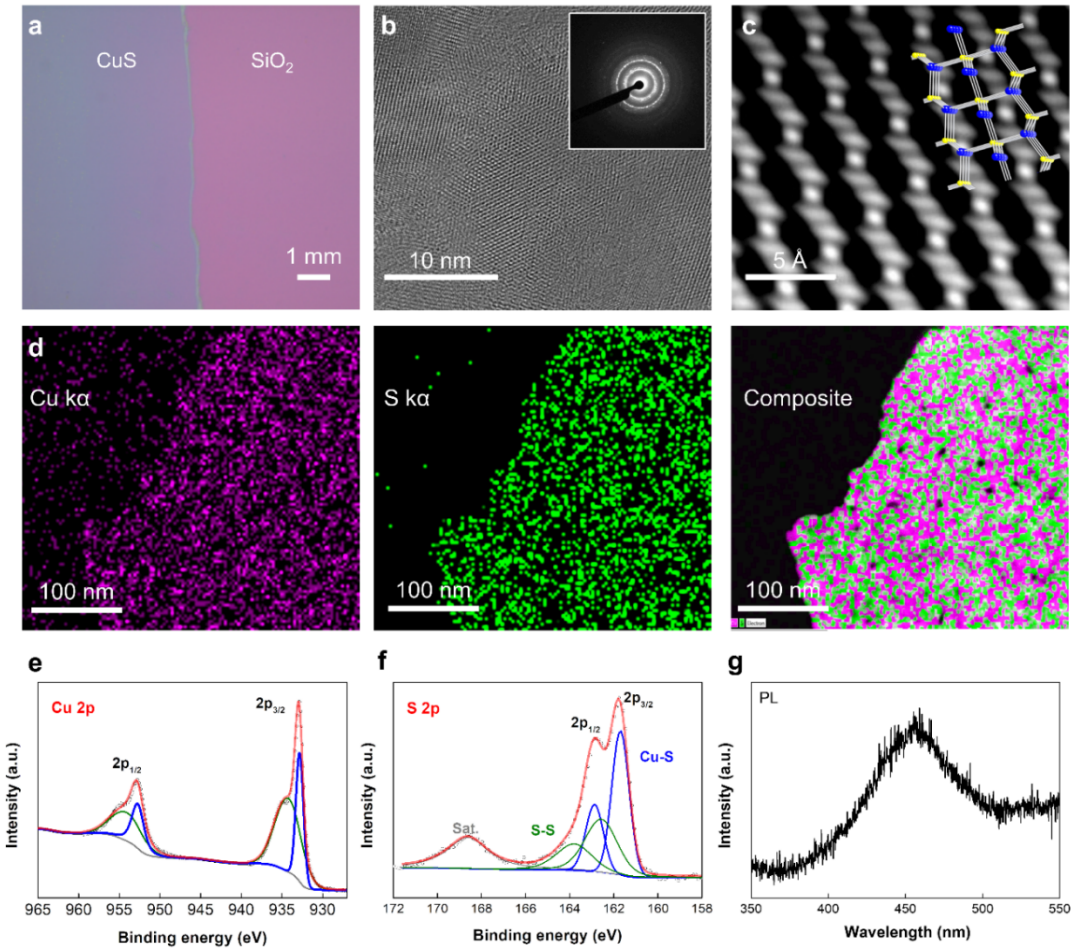

Figure 3. (a) Optical microscopy image of a CuS nanosheet on a SiO_2/Si substrate. (b) TEM image of CuS. Inset image shows an SAED image of CuS (c) ARM HAADF-STEM image of CuS. (d) Mapping images of Cu kα, S kα and composite of CuS. XPS spectra of (e) Cu 2p and (f) S 2p of CuS. (g) PL spectra of CuS.

The crystal nature of CuS was analyzed directly using atomic-resolution high-angle annular dark-field scanning transmission electron microscopy (ARM HAADF-STEM). **Figure 3**a shows the wet transferred CuS nanosheet films on a SiO_2 substrate. The nanosheets were further transferred onto a gold grid for TEM analysis. A well-organized honeycomb structure (**Figure** 3b),

along with corresponding spotty selected-area ring patterns (inset of **Figure** 3b) suggests that the atomically thin covellite crystal of the as-prepared CuS is indeed an atomically thin covellite crystal. Characteristic atomic-scale lattice images were taken through (100)-axis, which shows the consistent spatial distribution of the Cu and S atoms (**Figure** 3c) with the atomic covellite model (inset of **Figure** 3c). The stoichiometric phase distribution of CuS is determined through HAADF-STEM energy-dispersive X-ray spectroscopy mapping (**Figure** 3d), which exhibit a homogeneous distribution of the Cu and S elements over CuS. X-ray photoelectron spectroscopy (XPS) analysis was also carried out to further verify the chemical states of CuS (**Figure** S4). **Figures** 3e and 3f show the high-resolution XPS spectra of the S 2p and Cu 2p peak regions, respectively. The locations of the binding energy peaks of Cu 2p at 932.8 and 934.5 eV are indicative of the chemical states of CuS.[33]

The S 2p fitting peaks can be deconvoluted into two main deconvoluted doublets. The two main peak doublets are centered at 161.6 eV and 162.6 eV, which are typical values for metal sulfides and can be assigned to sulfide and disulfide, respectively, implying that the ionic model of the as-prepared nanosheets is $(Cu_2)^{2+}(Cu)^{2+}(S_2)^{2-}(S)^2$.[34] These findings also indicate that our samples have been successfully converted from cubic copper to covellite CuS with high crystalline quality. The optical properties of the CuS nanosheets were characterized by photoluminescence (PL, wavelength 266 nm, 20 mW) spectroscopy. **Figure** 3g represents the emission spectra of the 10nm-CuS sample. The emission peak is centered at ~ 450 nm, which is close to the reported PL emission peaks of bulk CuS and ultrathin CuS, demonstrating that, after the sulfurization process, the pure Cu is converted to the CuS composition.[35] The thickness of the CuS nanosheets were also characterized using an AFM as shown in **Figure** S5.

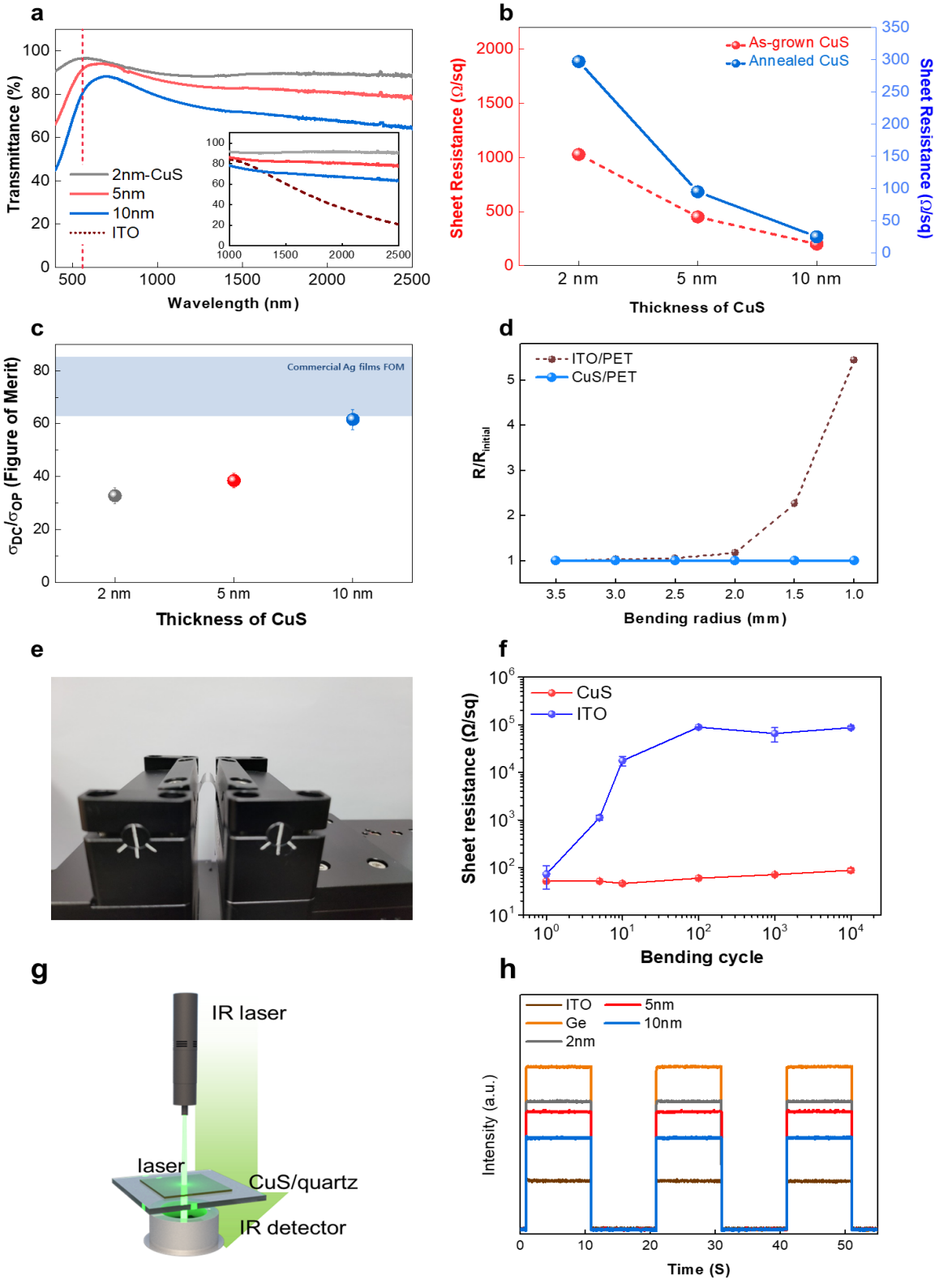
a
Transmittance (%)
Wavelength (nm)
2nm-CuS
5nm
10nm
ITO
b
Sheet Resistance (Ω/sq)
Sheet Resistance (Ω/sq)
As-grown CuS
Annealed CuS
Thickness of CuS
2 nm
5 nm
10 nm
c
σDC/σOP (Figure of Merit)
Commercial Ag films FOM
Thickness of CuS
d
R/Rinitial
ITO/PET
CuS/PET
Bending radius (mm)
e
f
Sheet resistance (Ω/sq)
CuS
ITO
Bending cycle
g
IR laser
laser
CuS/quartz
IR detector
h
ITO
5nm
Ge
10nm
2nm
Intensity (a.u.)
Time (S)

1

Figure 4. (a) Transmission spectrum of CuS and ITO films. Inset shows the transmittance curve of CuS and ITO films for just the IR region (b) Sheet resistance values of CuS nanosheet films before and after thermal treatment at 150 ^{0}C (c) FoM values for the 2 nm-, 5 nm- and 10 nm-CuS nanosheet films. (d) Sheet resistance of CuS and ITO electrodes for different bending radii. Inset images show that the CuS electrode can still function even when it is bended. (e) An optical image of a bending test machine. (f) Sheet resistance of CuS and ITO films after the 10,000 bending cycles. (g) Schematic illustration of the infrared laser penetration test. (h) On-off IR photoswitch curve for the CuS and ITO electrodes.

The electrical, optical and mechanical properties of the CuS film as a flexible and transparent conductive electrode were determined as shown in **Figure** 4. The optical transmittance of CuS on a glass substrate was measured using a spectrometer covering the visible to infrared region (450 nm to 2500 nm) (**Figure** 4a). The transmittance of CuS at 550 nm is clearly comparable to that of the ITO films, which are ~96.1%, ~90.7% and ~79.4% for the 2 nm-CuS, 5 nm-CuS and 10 nm-CuS films, respectively. Moreover, the CuS nanosheet films have superior transmittance in the infrared region from 1000 to 2500 nm (~ 80%). As shown in the inset of **Figure** 4a, the commercial ITO films have poor transmittance in this region (~ 40%) especially at 2000 nm. Based upon this optical property, CuS nanosheets are clearly an appealing candidate for optoelectronic devices in the visible to infrared region. Moreover, the transmittance of CuS in the visible region below 600nm drop sharply.[36-39]

Figure 4b shows the sheet resistance values for 2 nm-, 5 nm-, and 10 nm-CuS nanosheets using the four-point resistance measurement. The electrical conductivity of CuS dramatically

improved with increasing thickness, while the transparency decreased slightly from 2 nm- to 10 nm-CuS. The average sheet resistance values of CuS are found to be 297.2 Ω sq^{-1}, 94.9 Ω sq^{-1} and 25.1 Ω sq^{-1}, respectively, following thermal treatment at 150 ^{0}C for 5 min under inert gas (**Figure** S6). These high conductivity values correlate with the metallic-like properties of as-grown CuS. The further crystallization and atomic ordering of the as-prepared CuS can be induced by simple heat treatment at 150 ^{0}C. The calculated average figure of merits (FoMs) of the 2 nm-, 5 nm-, and 10 nm-CuS nanosheets at 550 nm are found to be 31.9, 39.8 and 61.6, respectively, which are higher than the industrial commercialization standard for optical applications (**Figure** 4c).[40] The FoMs in the IR region are much higher than that of commercial TCEs (usually less than 20). Commercial nano silver wire transparent conductive films (NSWTCFs) with a transparency of ~92% and a sheet resistance 50~70 Ω sq^{-1}were purchased and the electrical and mechanical properties of NSWTCF were tested to compare the performance of CuS (Figure S7). To investigate the electric stability of CuS under air exposure, the sheet resistances of the CuS and pure Cu films were examined. As shown in Figure S8a, on the basis of XRD results, the Cu_xO peaks were identified on the Cu films after few days under air. These partially oxidized films are not well crystallized. Moreover, in terms of electrical conductivity, as shown in Figure S8b, the CuS films can well maintain its original conductivity, but the conductivity of the as-deposited Cu films was dramatically decreased after 7 days

Mechanical and durability assessment of the CuS nanosheets was carried out by measuring the variation in the sheet resistance. The relative resistance values of the CuS and ITO films before and after bending were evaluated (**Figure** 4d). While the relative resistance of the ITO films drastically increased according to a decrease in the bending radius from 3.5 mm to 1.0 mm. The relative resistance of the CuS nanosheets remains nearly unchanged. Moreover, for the durability

test, the slope of the two terminal I-V curves was well-maintained even though the CuS nanosheet films were bended, twisted, and even crumpled (**Figures** S9a and 9b). The experimental results show that the CuS nanosheets possess good optical and electrical properties as well as superior bending properties with high degree of durability.

To investigate the mechanical stability of CuS, as shown in Figure 4e, the CuS and ITO films were folded 10,000 times using a home-made automatic fold testing machine, and the sheet resistances of both films were measured. As shown in Figure 4f, the resistance of the ITO films has been dropped dramatically after the 10,000 cycles. Instead, the CuS films can maintain its original sheet resistance even after the 10,000 folds, which demonstrating its superior mechanical stability of CuS against the applied stress. **Figure** 4g shows a schematic illustration of an IR light transmitting test using a 1550 nm incident laser on the film and a germanium (Ge)-IR detector. The initial intensity of the laser was compared with that of the incident laser after penetrating the CuS nanosheet films, ITO or glass substrates and the IR laser was turned on and off within a 10 sec time frame. Compared to the ITO films and glass, the readout intensity of the IR laser exhibited negligible attenuation after transmitting through the CuS nanosheets. A monotonic IR transmittance phenomena was observed in our thickness-dependent studies. As shown in **Figure** 4h, the thinnest CuS nanosheet film shows the highest IR transmittance beyond the others which indicates that the atomic-thick CuS nanosheet has negligible IR absorption or reflection. These results imply that the CuS electrodes can be potentially applied to IR optical and electronic applications as a promising electrode candidate.

To further examine the eligibility of the CuS nanosheets as one of the possible TCE in optical electronic applications, we fabricated cadmium selenide (CdSe)/zinc sulfide (ZnS) core/shell quantum dot light emitting diodes (QD-LEDs) using a CuS electrode as the anode (the

charge transfer layer). **Figure** S9c shows a schematic illustration of the QD-LEDs. On the CuS electrode, a 50 nm poly(ethylenedioxythiophene):polystyrene sulphonate(PEDOT:PSS) was used as the hole injection layer (HIL), a 50 nm poly[(9,9-dioctylfluorenyl-2,7-diyl)-co-(4,4-(N-(4-sec-butylphenyl)) diphenylamine)] (TFB) layer was used as the hole transfer layer (HTL). The red-colored CdSe/ZnS QD films (30 nm) were spin-coated onto the as-prepared substrate. Finally, a 100 nm zinc oxide (ZnO) was used as the electron transfer layer (ETL) and an Al cathode were deposited on the QD films. Currently, the optimization of experimental parameters such as the coating of the QDs and the deposition of various transfer layers on the CuS electrodes is still under investigation for enhanced electroluminescent performance such as the external quantum efficiency. Nevertheless, the experimental characterization and the device results strongly recommend the use of CuS nanosheets and the simple sulfurization process at room temperature would establish a useful route for future optoelectronic devices when flexibility is a key requirement. Figure S9d shows the additional lighting image for 10 nm CuS/QDLED under the characterization. Figure S9e-f shows the I-V and EQE curve of the device. The estimated maximum luminescence is 1240.0 cd m^{-2}. The electrical properties of the CuS samples were measured by Hall Effect technique with tungsten (W) electrode contacts in a square sample of the 1x1 cm^2 with Van der Pauw configuration. All the samples exhibited p-type behavior (Average carrier concentration: 2.47×10^{22} cm^{-3} & Average mobility: 1.28 cm^2 $V^{-1}s^{-1}$) and showed the semi-metal behavior (Table S1).

■ CONCLUSION

In conclusion, wafer-scale metallic CuS nanosheets with high transparency, conductivity and excellent flexibility have been synthesized directly onto various substrates via an atmospheric sulfur adsorption-corrosion reaction. The gas sulfurization process has been utilized to grow high-quality CuS sheets with atomic-thickness controllability (from monolayers of 2 nm to multilayers of 10 nm). We have demonstrated that the CuS electrodes show high optical transparency and conductivity with FoM values close to 60, which readily surpass the industrial commercialization requirements for optical applications. Moreover, the CuS electrodes can be successfully applied to various optical applications such as apertures for IR detectors and TCEs for QD-LEDs. Our findings are of significant importance in the development of new TCEs for flexible optoelectronic applications with scalable productivity.

■ MATERIALS AND METHODS

Synthesis of CuS Nanosheets. Before sulfurization process, pure copper (Cu) films with different thicknesses were deposited on a Si/SiO_2 substrate, a glass or a flexible polyethylene terephthalate (PET) polymer substrate by thermal evaporation in high vacuum. The thicknesses of the Cu films were carefully tailored by a deposition meter in the machine. The deposited Cu films were directly exposed to the vaporized sulfur gas from an ammonium sulfide solution (20 wt.%) which was purchased from Sigma-Aldrich followed by 1~3 min of static displacement above the solution according to the thicknesses of CuS without any heat treatment in a lab environment at 25 °C. For the further conductive enhancement and crystallization, the CuS nanosheet films on the substrate were placed in the CVD furnace under Ar and annealed at 150 ºC for 1~5 min according to the desired thickness of CuS with rapid cooling processes.

Material and Electrical Characterization. The optical and crystal properties of CuS nanosheets were characterized using scanning electron microscopy (SEM, Hitachi S-4300), transmission electron microscopy (TEM, JEOL JEM-2200MCO FEGTEM), ultraviolet–visible spectroscopy (UV-Vis, Varian Cary 5000), Raman spectroscopy (Horiba LabRAM ARAMIS Imaging Confocal Raman Microscope), time of flight secondary ion mass spectrometry (TOF-SIMS-5,Germany), atomic force microscope (AFM, Veeco Dimension 3100) photoluminescence spectroscopy (PL, Fluorolog, Horiba Jobin Yvon) and high-resolution X-ray diffraction (XRD, Rigaku Medel Smartlab). To check the oxidation states of CuS, X-ray photon electron spectroscopy (XPS) was conducted using a Thermo Scientific K-Alpha XPS instrument with a micro-focused monochromatic Al X-ray source. The spectrometer was adjusted to align to a binding energy of 284.5 eV for the C 1s. The (opto)electronic properties of the CuS nanosheets and corresponding devices were measured using the electrical characterization system (4200-SCS, Keithley), LeCroy

HD4000 high-definition oscilloscope, and 6-probe Cascade Microtech probe station.

■ ACKNOWLEDGEMENT

This work was supported by the National Research Foundation (NRF) of Korea (2019R1A2C1005930), and the European Research Council under the European Union's Seventh Framework Programme (FP/2007-2013)/Grant Agreement no. 685758.

■ ASSOCIATED CONTENT

Supporting Information

Photographs and optical images of CuS, Raman spectra, SIMS spectra, XRD, AFM, XPS, AFM Height profiles, Sheet resistance values for 2 nm-, 5 nm- and 10 nm-CuS, Sheet resistances of commercial NSWTCF, Time-dependent sheet resistance of Cu and CuS, Schematic illustration of QD-LED with CuS, and I-V and EQE curve for CuS-10 nm/QD-LED

■ AUTHOR INFORMATION

Corresponding author

SeungNam Cha, *E-mail address: chasn@skku.edu, Tel: +82-31-299-4546

ORCID

John Hong: 0000-0002-1513-8622

Bo Hou: 0000-0001-9918-8223

Sangyeon Pak: 0000-0003-1765-3043

Taehun Kim: 0000-0002-3695-4071

A-Rang Jang: 0000-0002-0758-9757

Yuljae Cho: 0000-0003-2976-0604

Sanghyo Lee: 0000-0002-4723-9612

Geon-Hyoung An: 0000-0003-0211-7993

Jae Eun Jang: 0000-0002-8523-1785

Stephen M. Morris: 0000-0001-8294-9225

Jung Inn Sohn: 0000-0002-3155-4327

SeungNam Cha: 0000-0001-6284-8312

Author Contributions

† John Hong, Byung-Sung Kim, Bo Hou contributed equally to the work

■ REFERENCES

[1] Allen, M.; Tung, V.; Kaner, R. Honeycomb Carbon: A Review of Graphene. *Chem. Rev.* **2010**, *110*, 132-145.

[2] Das, S.; Robinson, J.; Dubey, M.; Terrones, H.; Terrones, M. Beyond Graphene: Progress in Novel Two-Dimensional Materials and van der Waals Solids. *Annu. Rev. Mater. Res.* **2015**, *45*, 1-27.

[3] Zhang, K.; Feng, Y.; Wang, F.; Yang, Z.; Wang, J. Two-Dimensional Hexagonal Boron Nitride (2D-hBN): Synthesis, Properties and Applications. *J. Mater. Chem. C* **2017**, *5*, 11992-12022.

[4] Liu, H.; Hu, K.; Yan, D.; Chen, R.; Zou, Y.; Liu, H.; Wang, S. Recent Advances on Black Phosphorus for Energy Storage, Catalysis, and Sensor Applications. *Adv. Mater.* **2018**, *30*, 1800295 (1-22).

[5] Wang, Q. H.; Kalantar-Zadeh, K.; Kis, A.; Coleman, J.; Strano, M. Electronics and Optoelectronics of Two-Dimensional Transition Metal Dichalcogenides. *Nat. Nanotechnol.* **2012**, *7*, 699-712.

[6] Shi, S.; Sun, Z.; Hu, Y. H. Synthesis, Stabilization and Applications of 2-Dimensional 1T Metallic MoS_2 *J. Mater. Chem. A* **2018**, *6*, 23932-23977.

[7] Anasori, B.; Lukatskaya, M.; Gogotsi, Y. 2D Metal Carbides and Nitrides (MXenes) for Energy Storage. *Nat. Rev. Mater.* **2017**, *2*, 16098 (1-17).

[8] Yoon, J.; Park, W.; Bae, G.-Y.; Kim, Y.; Jang, H. S.; Hyun, Y.; Lim, S. K.; Kahng, Y. H.; Hong, W.-K.; Lee, B. H.; Ko, H. C. Highly Flexible and Transparent Multilayer MoS_2 Transistors with Graphene Electrodes. *Small* **2013**, *9*, 3295 (1-6).

[9] Kuzum, D.; Takano, H.; Shim, E.; Reed, J.; Juul, H.; Richardson, A.; Vries, J.; Bink, H.; Dichter, M.; Lucas, T.; Coulter, D.; Cubukcu, E.; Litt, B. Transparent and Flexible Low Noise Graphene Electrodes for Simultaneous Electrophysiology and Neuroimaging. *Nat. Commun.* **2014**, *5*, 5259 (1-10).

[10] Rana, K.; Singh, J.; Ahn, J.-H. A Graphene-Based Transparent Electrode for Use in Flexible Optoelectronic Devices. *J. Mater. Chem. C* **2014**, *2*, 2646-2656.

[11] Tan, R. K. L.; Reeves, S.; Hashemi, N.; Thomas, D. G.; Kavak, E.; Montazami, R.; Hashemi, N. Graphene as a Flexible Electrode: Review of Fabrication Approaches. *J. Mater. Chem. A* **2017**, *5*, 17777-17803.

[12] Liu, L.; Wu, J.; Wu, L.; Ye, M.; Liu, X.; Wang, Q.; Hou, S.; Lu, P.; Sun, L.; Zheng, J.; Xing, L.; Gu, L.; Jiang, X.; Xie, L.; Jiao, L. Phase-selective Synthesis of 1T' MoS_2 Monolayers and Heterophase Bilayers. *Nat. Mater.* **2018**, *17*, 1108-1114.

[13] Rao, C. N. R.; Matte, H. S. S.; Subrahmanyam, K. S. Synthesis and Selected Properties of Graphene and Graphene Mimics. *Acc. Chem. Res.* **2013**, *46*, 149-159.

[14] Suk, J. W.; Kitt, A.; Magnuson, C.; Hao, Y.; Ahmed, S.; An, J.; Swan, A.; Goldberg, B.; Ruoff, R. Transfer of CVD-Grown Monolayer Graphene onto Arbitrary Substrates *ACS Nano* **2011**, *5*, 6916-6924.

[15] Hong, J.; Kim, B.-S.; Yang, S.; Jang, A.-R.; Lee, Y.-W.; Pak, S.; Lee, S.; Cho, Y.; Kang, D.; Shin, H. S.; Hong, J. P.; Morris, S.; Cha, S.; Sohn, J. I.; Kim, J. M. Chalcogenide Solution-Mediated Activation Protocol for Scalable and Ultrafast Synthesis of Single-Crystalline 1-D Copper Sulfide for Supercapacitors. *J. Mater. Chem. A* **2019**, *7*, 2529-2535.

[16] Roy, P.; Srivastava, S. K. Nanostructured Copper Sulfides: Synthesis, Properties and Applications. *Crystengcomm*. **2015**, *17*, 7801-7815.

[17] Sun, S.; Li, P.; Liang, S.; Yang, Z. Diversified Copper Sulfide ($Cu_{2-x}S$) Micro-/Nanostructures: A Comprehensive Review on Synthesis, Modifications and Applications *Nanoscale* **2017**, *9*, 11357-11404.

[18] Mousavi-Kamazani, M.; Zarghami, Z.; Salavati-Niasari, M. Facile and Novel Chemical Synthesis, Characterization, and Formation Mechanism of Copper Sulfide (Cu_2S, Cu_2S/CuS, CuS) Nanostructures for Increasing the Efficiency of Solar Cells. *J. Phys. Chem. C* **2016**, *120*, 2096-2108.

[19] Nozaki, H.; Shibata, K.; Ohhashi, N. Metallic Hole Conduction in CuS. *J. Solid. State. Chem*. **1991**, *91*, 306-311.

[20] Soares, A.; Santos, E.; Morales-Garcia, A.; Heine, T.; Abreu, H.; Duarte, H. Two-Dimensional Crystal CuS—Electronic and Structural Properties. *2D Mater*. **2017**, *4*, 015041 (1-7).

[21] Lee, Y.-W.; Kim, B.-S.; Hong, J.; Lee, J.; Pak, S.; Jang, H.-S.; Whang, D.; Cha, S.; Sohn, J. I.; Kim, J. M. A Pseudo-Capacitive Chalcogenide-based Electrode with Dense 1-Dimensional Nanoarrays for Enhanced Energy Density in Asymmetric Supercapacitors. *J. Mater. Chem. A* **2016**, *4*, 10084-10090.

[22] Sakamoto, T.; Sunamura, H.; Kawaura, H.; Hasegawa, T.; Nakayama, T.; Aono, M. Nanometer-Scale Switches Using Copper Sulfide *Appl. Phys. Lett*. **2003**, *82*, 3032-3034.

[23] Bitla, Y.; Chen, C.; Lee, H.-C.; Do, T. H.; Ma, C.-H.; Qui, L. V.; Huang, C.-W.; Wu, W.-W.; Chang, L.; Chiu, P.-W.; Chu, Y.-H. Oxide Heteroepitaxy for Flexible Optoelectronics. *ACS Appl. Mater. Interfaces* **2016**, *8*, 32401-32407.

[24] Graedel, T. E.; Franey, J. P.; Gualtieri, G. J.; Kammlott, G. W.; Malm, D. L. On the Mechanism of Silver and Copper Sulfidation by Atmospheric H_2S and OCS. *Corros. Sci.* **1985**, *25*, 1163-1180.

[25] Galtayries, A.; Bonnelle, J.-P. XPS and ISS Studies on the Interaction of H_2S with Polycrystalline Cu, Cu_2O and CuO Surfaces. *Surf. Interface Anal.* **1995**, *23*, 171-179.

[26] Reid, M.; Punch, J.; Ryan, C.; Garfias, L. F.; Belochapkine, S.; Franey, J. P.; Derkits, G. E.; Reents, W. D. Microstructural Development of Copper Sulfide on Copper Exposed to Humid H_2S. *J. Electrochem. Soc.* **2007**, *154*, C209-C214.

[27] Sansregret, J. L. Reaction of Copper Oxide with H_2S. *J. Electrochem. Soc.* **1980**, 1, 2083.

[28] Adhikari, S.; Sarkar, D.; Madras, G. Hierarchical Design of CuS Architectures for Visible Light Photocatalysis of 4-Chlorophenol. *ACS Omega* **2017**, *2*, 4009-4021.

[29] Minceva-Sukarova, B.; Najdoski, M.; Grozdanov, I.; Chunnilall, C. J. Raman Spectra of Thin Solid Films of Some Metal Sulfides *J. Mol. Struct.* **1997**, *410-411*, 267-270.

[30] Kumar, P.; Nagarajan, R. An Elegant Room Temperature Procedure for the Precise Control of Composition in the Cu–S System. *Inorg. Chem.* **2011**, *50*, 9204-9206.

[31] Mondal, G.; Bera, P.; Santra, A.; Jana, S.; Mandal, T. N.; Mondal, A.; Seok, S. I.; Bera, P. *New J. Chem*. Precursor-Driven Selective Synthesis of Hexagonal Chalcocite (Cu_2S) Nanocrystals: Structural, Optical, Electrical and Photocatalytic Properties. **2014**, *38*, 4774-4782.

[32] Huang, K.-J.; Zhang, J.-Z.; Fan, Y. One-Step Solvothermal Synthesis of Different Morphologies CuS Nanosheets Compared as Supercapacitor Electrode Materials. *J. Alloy. Compd*. **2015**, *625*, 158-163.

[33] Karikalan, N.; Karthik, R.; Chen, S.-M.; Karuppiah, C.; Elangovan, A. Sonochemical Synthesis of Sulfur Doped Reduced Graphene Oxide Supported CuS Nanoparticles for the Non-Enzymatic Glucose Sensor Applications. *Sci. Rep*. **2017**, *7*, 2494 (1-10).

[34] Estrada, A.; Silva, F.; Soares, S.; Coutinho, J.; Trindade, T. An Ionic Liquid Route to Prepare Copper Sulphide Nanocrystals Aiming at Photocatalytic Applications. *RSC Adv*. **2016**, *6*, 34521-34528.

[35] Du, Y.; Yin, Z.; Zhu, J.; Huang, X.; Wu, X.-J.; Zheng, Z.; Yan, Q; Zhang, H. A General Method for the Large-scale Synthesis of Uniform Ultrathin Metal Sulphide Nanocrystals. *Nat. Commun*. **2012**, *3*, 1177 (1-7).

[36] Cruz, J.; Hernandez, S. A.; Delgado, F.; Angel, O.; Perez, R.; Delgado, G. Optical and Electrical Properties of Thin Films of CuS Nanodisks Ensembles Annealed in a Vacuum and Their Photocatalytic Activity. *Int. J. Photoenergy* **2013,** *2013*, 178017 (1-9).

[37] Jia, L.; Lai, J.; Wang, J.; Chen, H.; Zheng, X.; Liu, H.; Jin, Z. Morphology, Structure and Optical Absorption Properties of Copper Sulfides by Different TEG Based Solution Processing. *Mater. Des.* **2017,** *123*, 39-45.

[38] Li, S.; Zha, T.; Wang, Q; Wang, C.; Ren, Y.; Chen, Y.; Pan, D. Facile Fabrication of p-Type Cu_xS Transparent Conducting Thin Films by Metal Sulfide Precursor Solution Approach and Their Application in Quantum Dot Thin Films. *J. Alloys Compd.* **2017,** *716*, 278-283.

[39] Dexter, M.; Gao, Z.; Bansal, S.; Chang, C.-H.; Malhotra, R. Temperature, Crystalline Phase and Influence of Substrate Properties in Intense Pulsed Light Sintering of Copper Sulfide Nanoparticle Thin Films. *Sci. Rep.* **2018,** *8*, 2201.

[40] Ellmer, K. Past Achievements and Future Challenges in the Development of Optically Transparent Electrodes. *Nat. Photonics* **2012**, *6*, 809-817.

Table of Contents